Electronic Supplementary Information

Monolithic porous carbon membrane-based hybrid electrodes with ultrahigh mass loading carbon-encapsulated Co nanoparticles for high-performance supercapacitors

Zhicheng Wei,[a,b,c] Zhengguo Zhang,[a,b,c] Fang Wang,[a,b,c] Shixiong Min*[a,b,c]

[a]*School of Chemistry and Chemical Engineering, North Minzu University, Yinchuan, 750021, P. R. China.*

[b]*Key Laboratory of Chemical Engineering and Technology, State Ethnic Affairs Commission, North Minzu University, Yinchuan, 750021, P. R. China.*

[c]*Ningxia Key Laboratory of Solar Chemical Conversion Technology, North Minzu University, Yinchuan 750021, P. R. China.*

*Corresponding authors: sxmin@nun.edu.cn

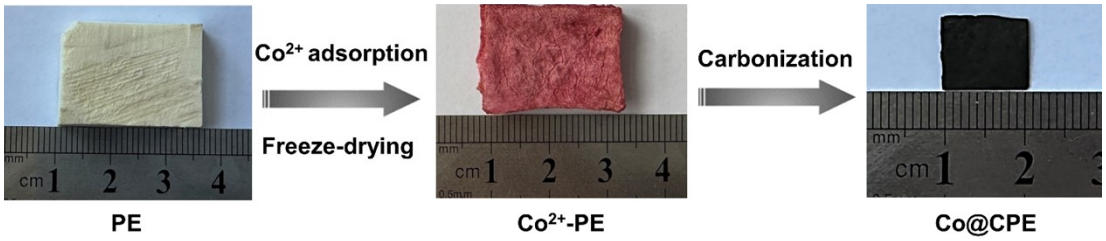

Fig. S1 Photographs showing the fabrication process of the Co@CPE electrodes.

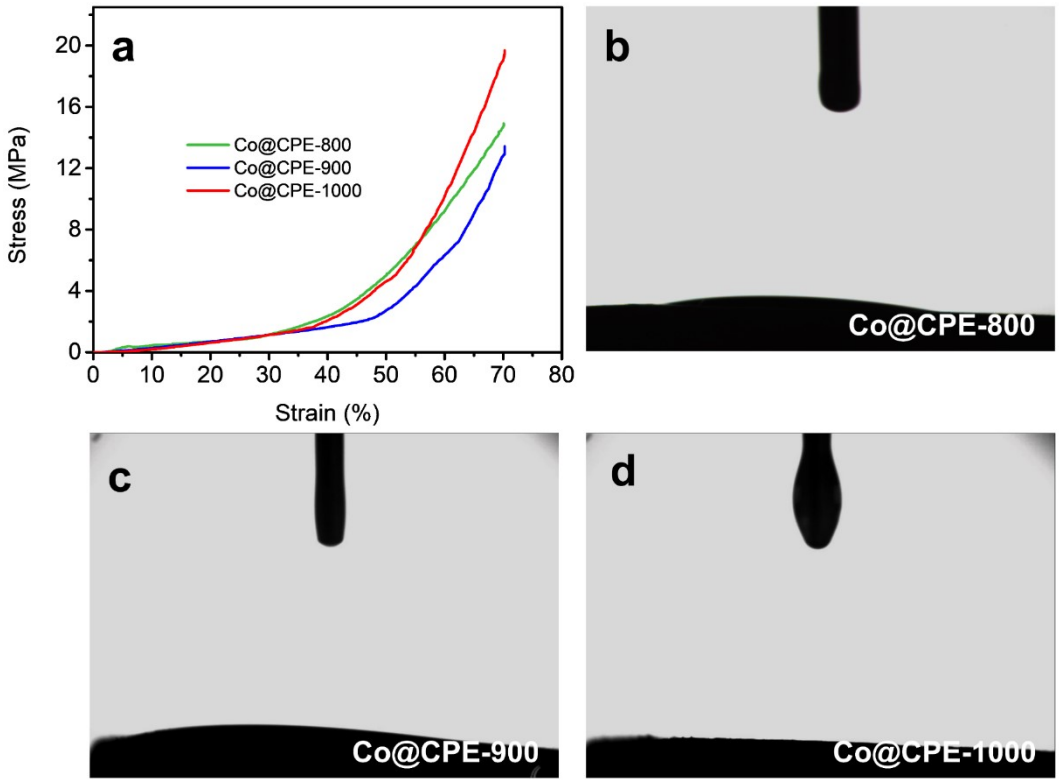

Fig. S2 (a) Compressive stress-strain curves and (b, c, and d) electrolyte wettability tests of the Co@CPE electrodes.

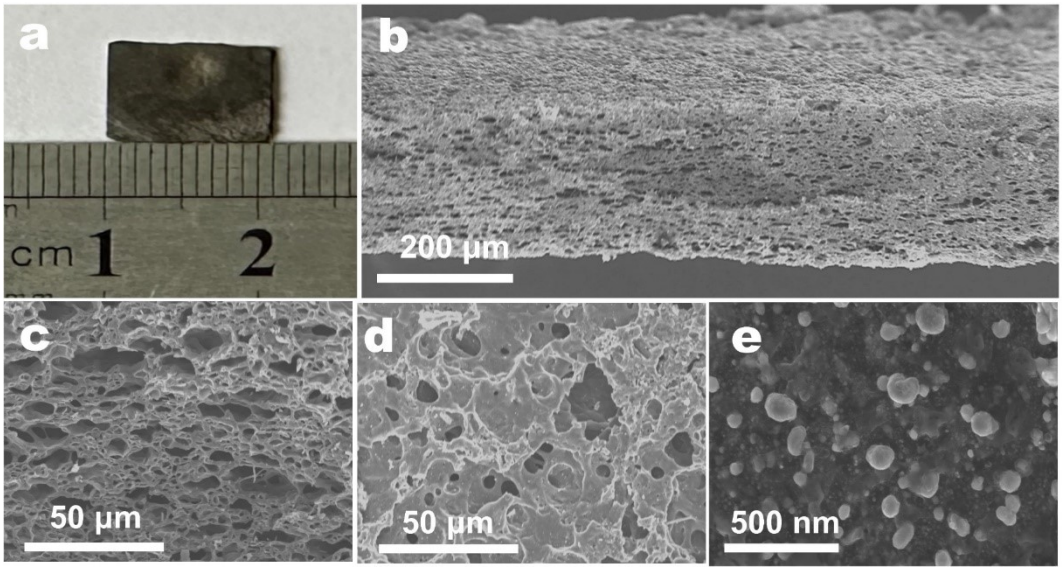

Fig. S3 (a) Photograph Co@CPE-800 electrode. (b) SEM image showing the overall view of Co@CPE-800 electrode. SEM images of (c) cross section and (d) top surface of Co@CPE-800 electrode. (e) High-magnification SEM image of Co@CPE-800 electrode.

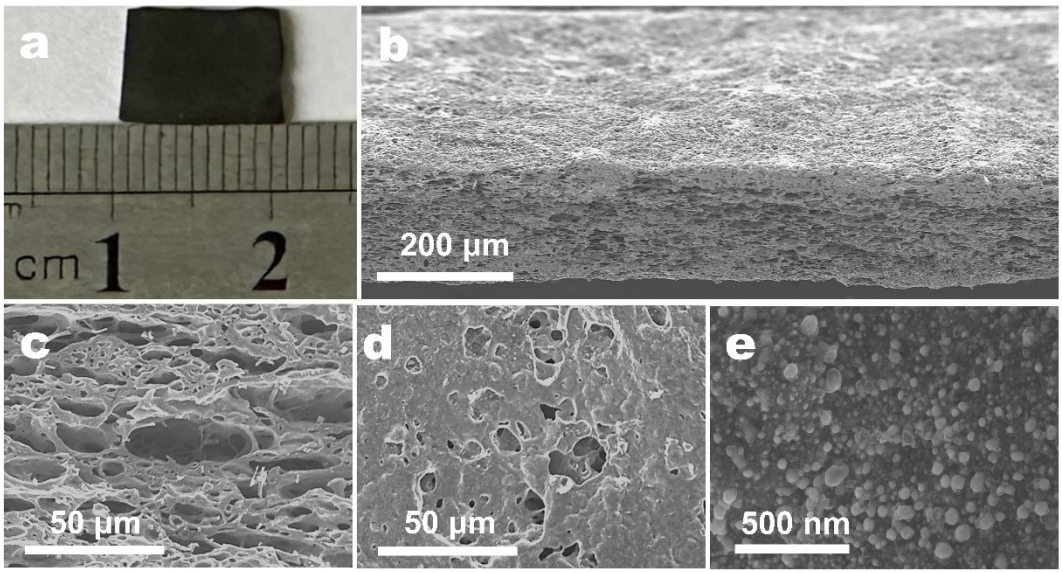

Fig. S4 (a) Photograph Co@CPE-900 electrode. (b) SEM image showing the overall view of Co@CPE-900 electrode. SEM images of (c) cross section and (d) top surface of Co@CPE-900 electrode. (e) High-magnification SEM image of Co@CPE-900 electrode.

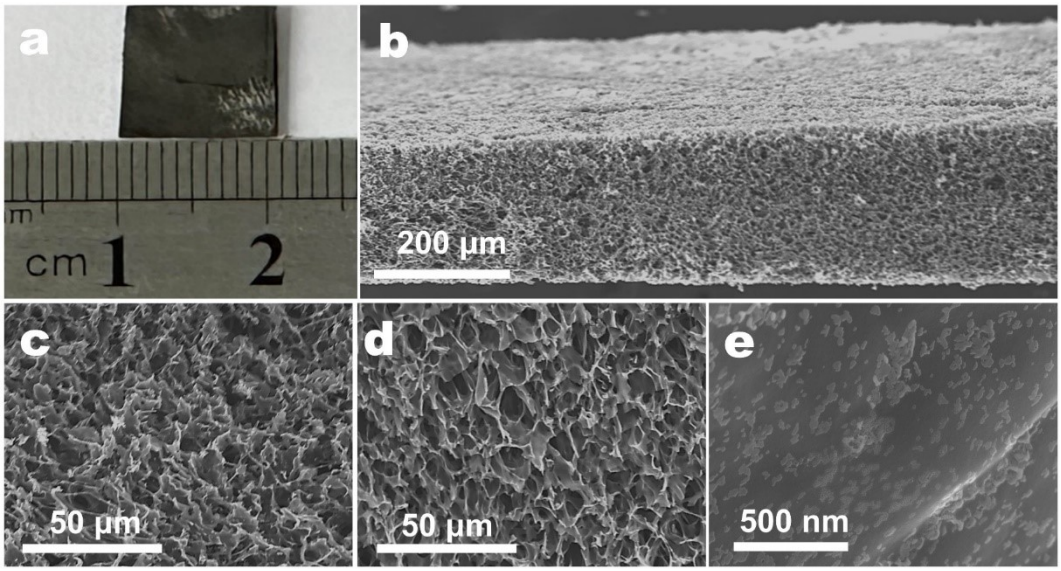

Fig. S5 (a) Photograph CPE-800 electrode. (b) SEM image showing the overall view of CPE-800 electrode. SEM images of (c) cross section and (d) top surface of CPE-800 electrode. (e) High-magnification SEM image of CPE-800 electrode.

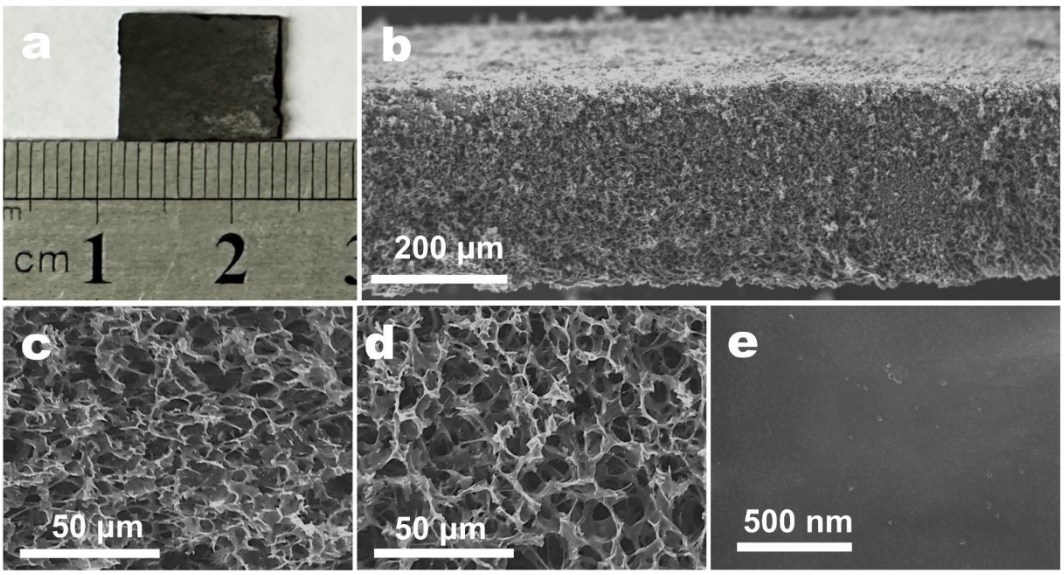

Fig. S6 (a) Photograph CPE-900 electrode. (b) SEM image showing the overall view of CPE-900 electrode. SEM images of (c) cross section and (d) top surface of CPE-900 electrode. (e) High-magnification SEM image of CPE-900 electrode.

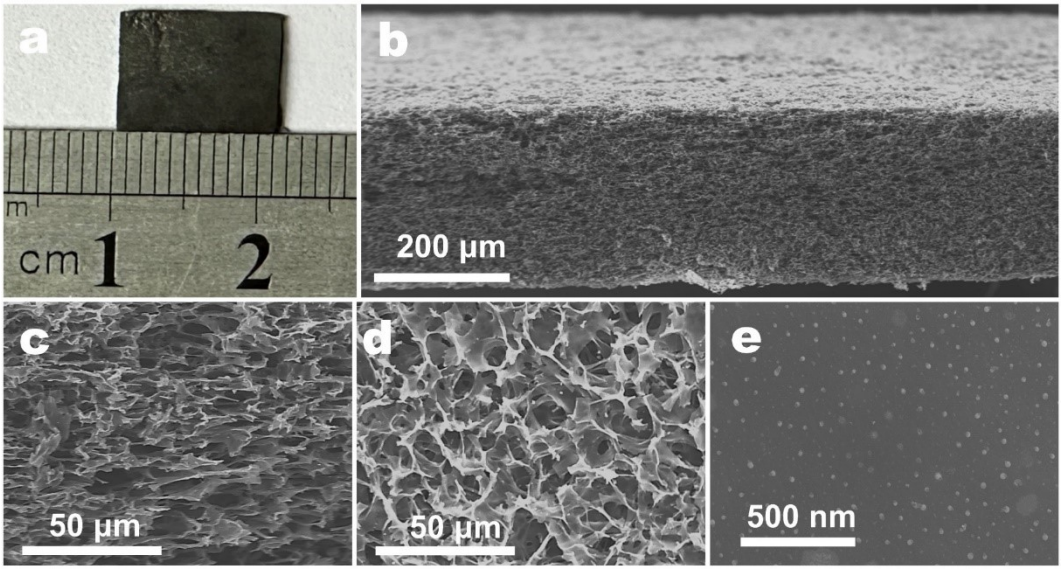

Fig. S7 (a) Photograph CPE-1000 electrode. (b) SEM image showing the overall view of CPE-1000 electrode. SEM images of (c) cross section and (d) top surface of CPE-1000 electrode. (e) High-magnification SEM image of CPE-1000 electrode.

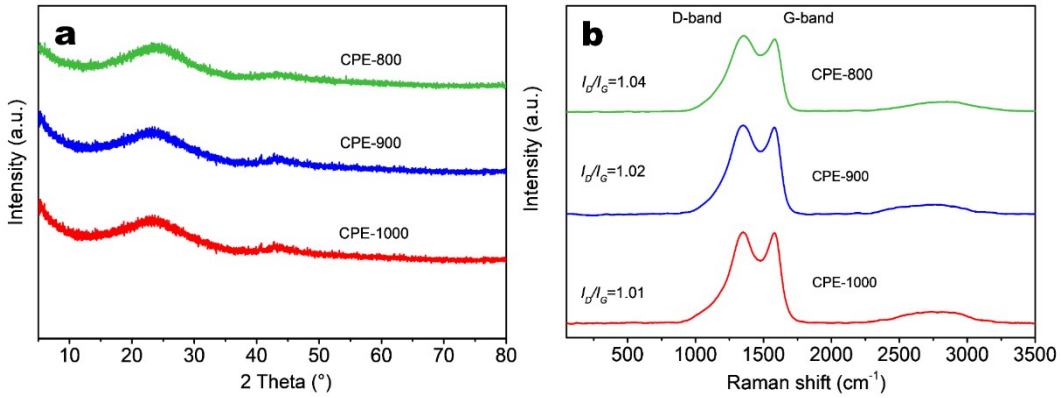

Fig. S8 (a) XRD patterns and (b) Raman spectra of the CPE electrodes.

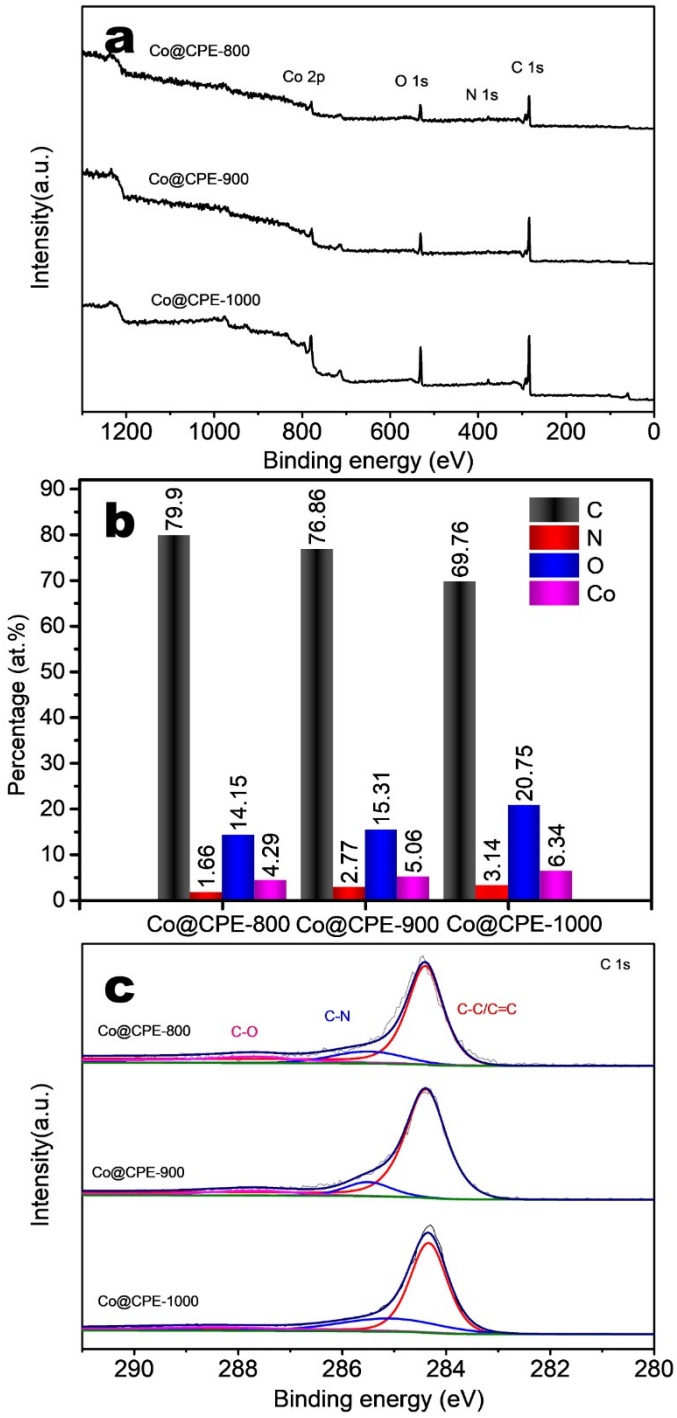

Fig. S9 (a) XPS survey spectra of the Co@CPE electrodes. (b) The percentages of C, O, N, and Co elements of the Co@CPE electrodes. (c) C 1s XPS spectra of the Co@CPE electrodes.

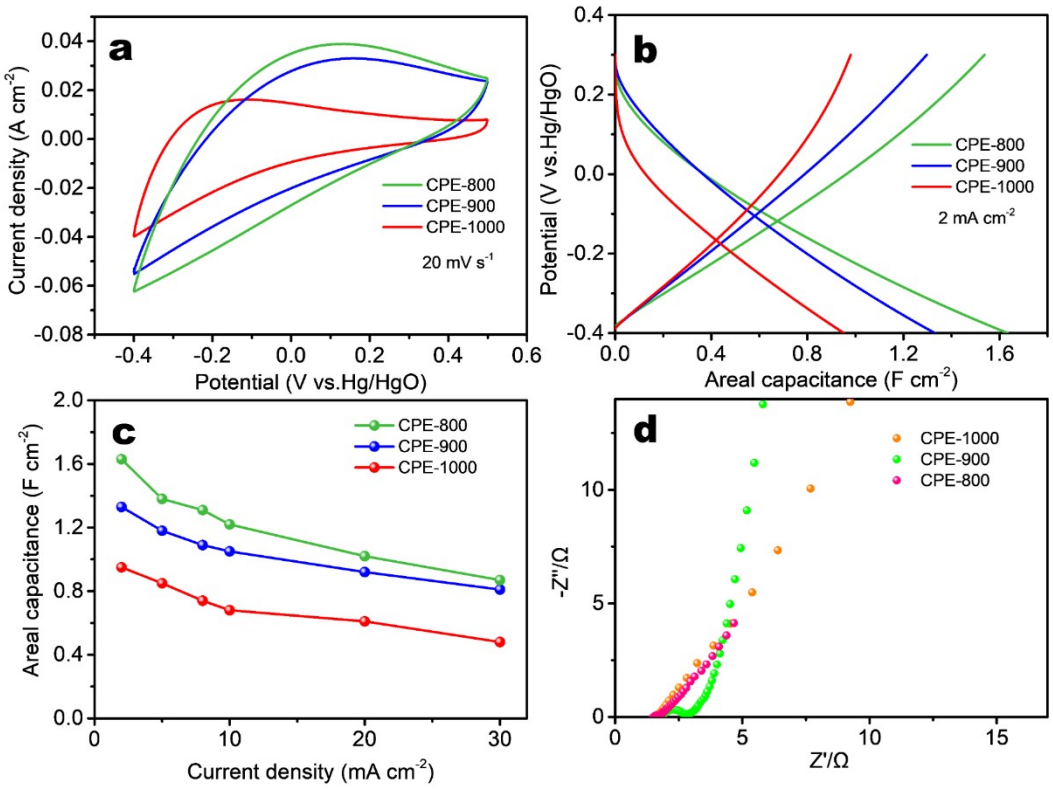

Fig. S10 (a) CV curves and (b) GCD curves of the CPE electrodes. (c) The areal capacitances of the CPE electrodes at different current densities. (d) EIS Nyquist plots of the CPE electrodes.

Table S1 Comparison of electrochemical performance of the Co@CPE-1000 electrode with those of previously reported transition metal-based electrodes.

Electrode material	Electrolyte	C_a (F cm^{-2})	Cycling stability	Ref
Co-MOF/NF	2 M KOH	13.6 F cm^{-2} (2 mA cm^{-2})	69.7% (2000 cycles)	1
Co-MOF/NF	3 M KOH	0.24 F cm^{-2} (0.5 mA cm^{-2})	70% (1500 cycles)	2
Co-Zn, Co-Cu(NF)	6 M KOH	2.39 F cm^{-2} (5 mA cm^{-2})	76.5 % (3000 cycles)	3
Co-PC@MX-CNF	2 M KOH	0.11 F cm^{-2} (2 mA cm^{-2})	90.36% (10000 cycles)	4
Fe-Co/NPC	6 M KOH	0.9 F cm^{-2} (10 mA cm^{-2})	88% (5000 cycles)	5
$Ni(OH)_2$@Co/C	1 M KOH	1.73 F cm^{-2} (1 mA cm^{-2})	97.3% (1000 cycles)	6
Co@C/Gro	6 M KOH	0.8 F cm^{-2} (0.5 mA cm^{-2})	87.3% (10000 cycles)	7
NiTe:Co(NF)	3 M KOH	2.96 F cm^{-2} (2 mA cm^{-2})	95% (5000 cycles)	8
Co-MOF/CC	2 M KOH	1.17 F cm^{-2} (1 mA cm^{-2})	94% (20000 cycles)	9
Ni/Co-MOF@CS	1 M KOH	2.04 F cm^{-2} (2.5 mA cm^{-2})	73% (5000 cycles)	10
Co-MOFs/NF	3 M KOH	3.83 F cm^{-2} (2 mA cm^{-2})	92.3% (3000 cycles)	11
Co@CPE-1000	6 M KOH	5.04 F cm^{-2} (2 mA cm^{-2})	113% (40000 cycles)	This work

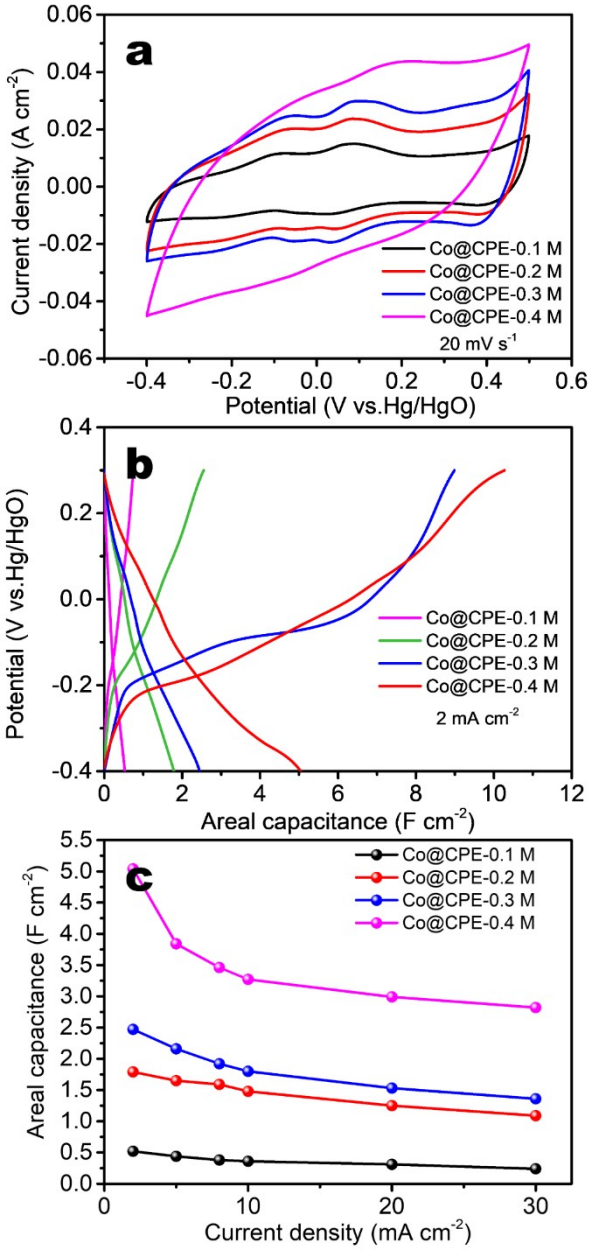

Fig. S11 (a) CV curves, (b) GCD curves, and (c) areal capacitances of the Co@CPE-1000 electrodes prepared using different concentrations of Co salt.

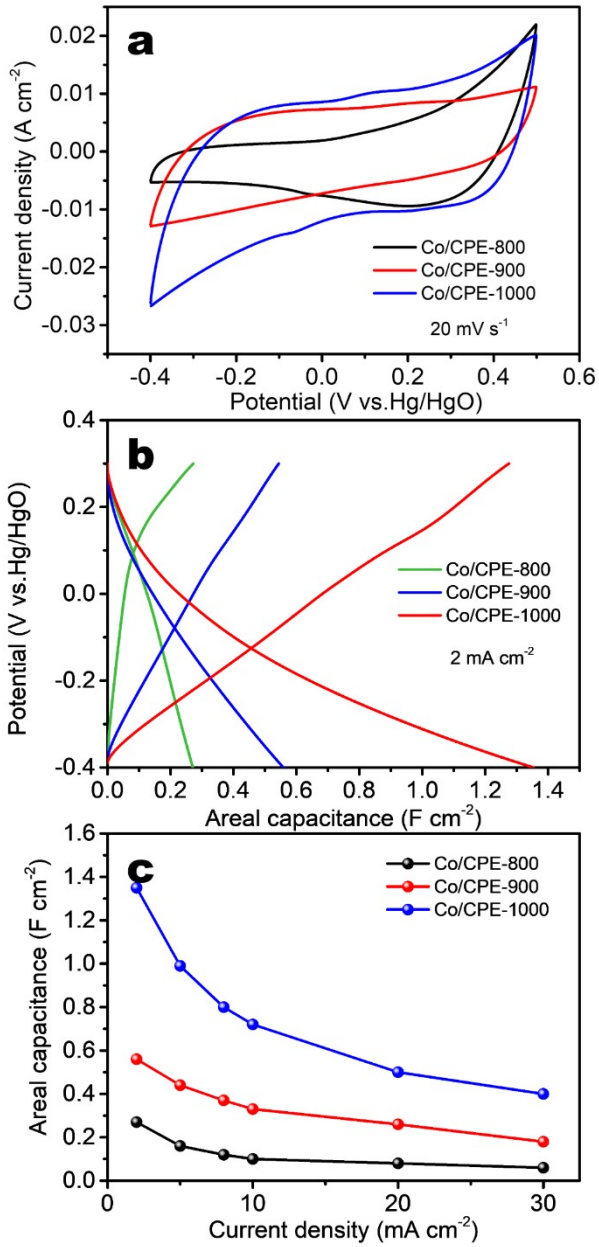

Fig. S12 (a) CV curves, (b) GCD curves, and (c) areal capacitances of the physically mixed Co/CPE electrodes.

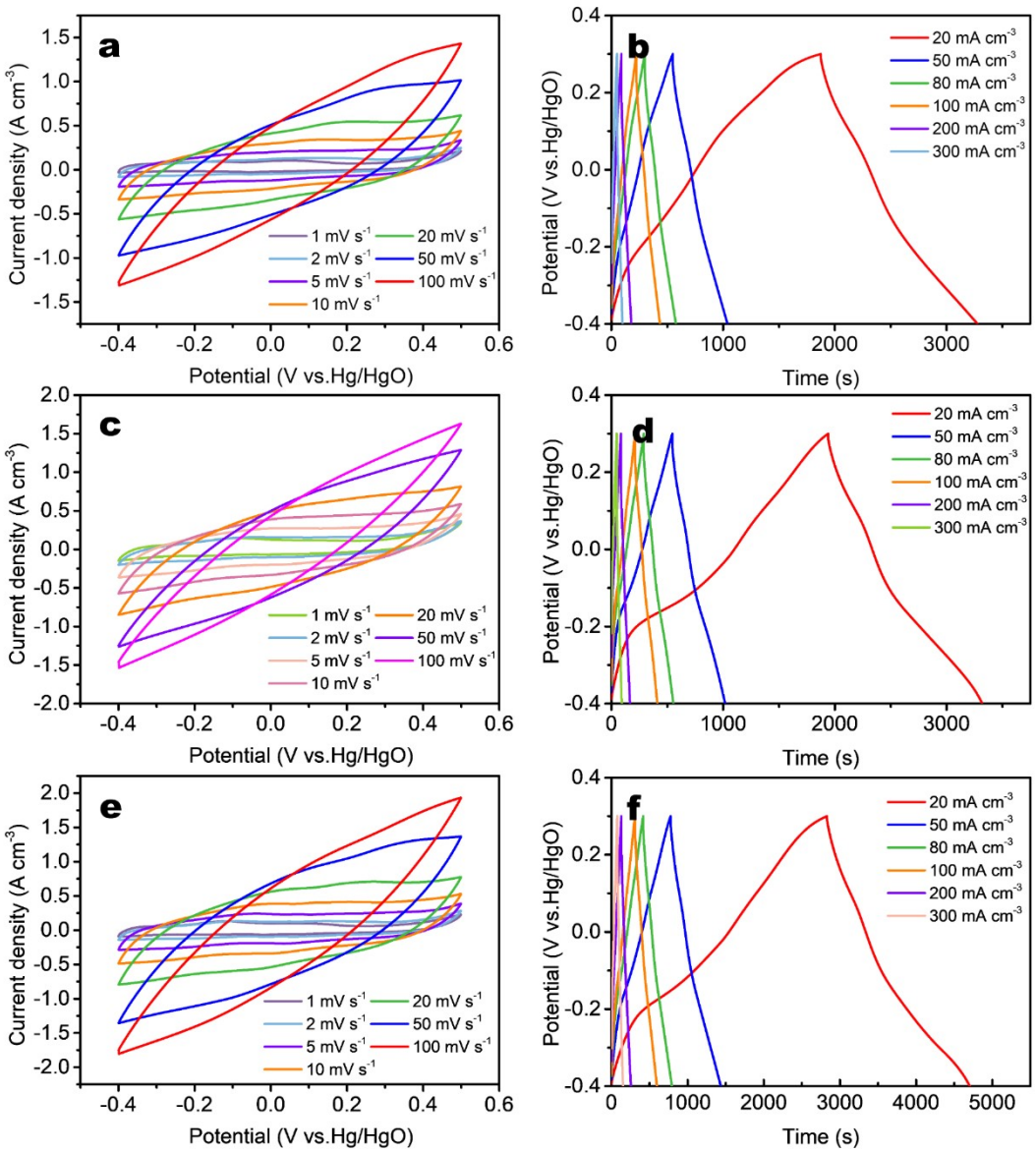

Fig. S13 (a) CV curves of Co@CPE-800 electrode at different scan rates. (b) GCD curves of Co@CPE-800 electrode at different current densities. (c) CV curves of Co@CPE-900 electrode at different scan rates. (d) GCD curves of Co@CPE-900 electrode at different current densities. (e) CV curves of Co@CPE-1000 electrode at different scan rates. (f) GCD curves of Co@CPE-1000 electrode at different current densities.

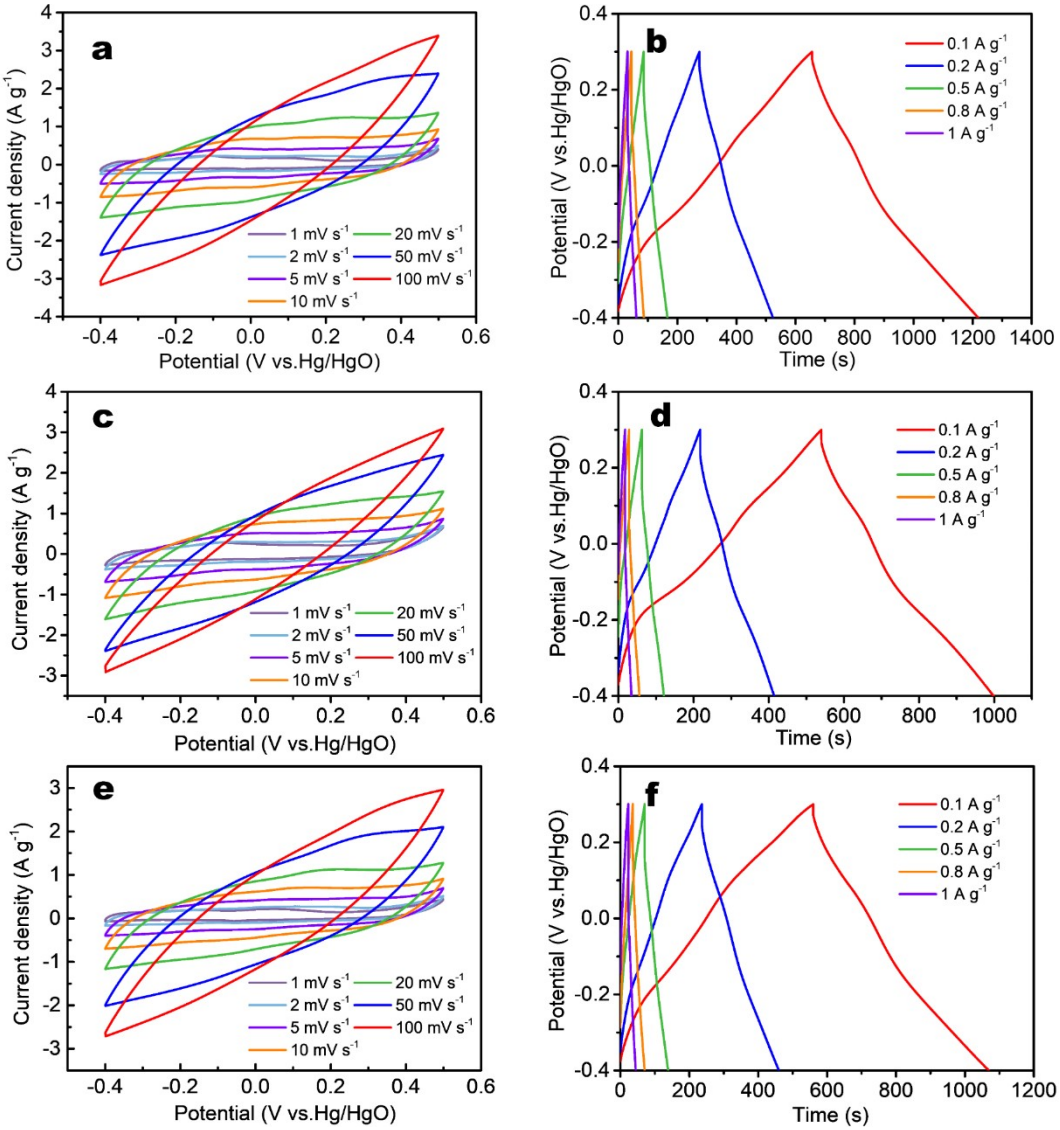

Fig. S14 (a) CV curves of Co@CPE-800 electrode at different scan rates. (b) GCD curves of Co@CPE-800 electrode at different current densities. (c) CV curves of Co@CPE-900 electrode at different scan rates. (d) GCD curves of Co@CPE-900 electrode at different current densities. (e) CV curves of Co@CPE-1000 electrode at different scan rates. (f) GCD curves of Co@CPE-1000 electrode at different current densities.

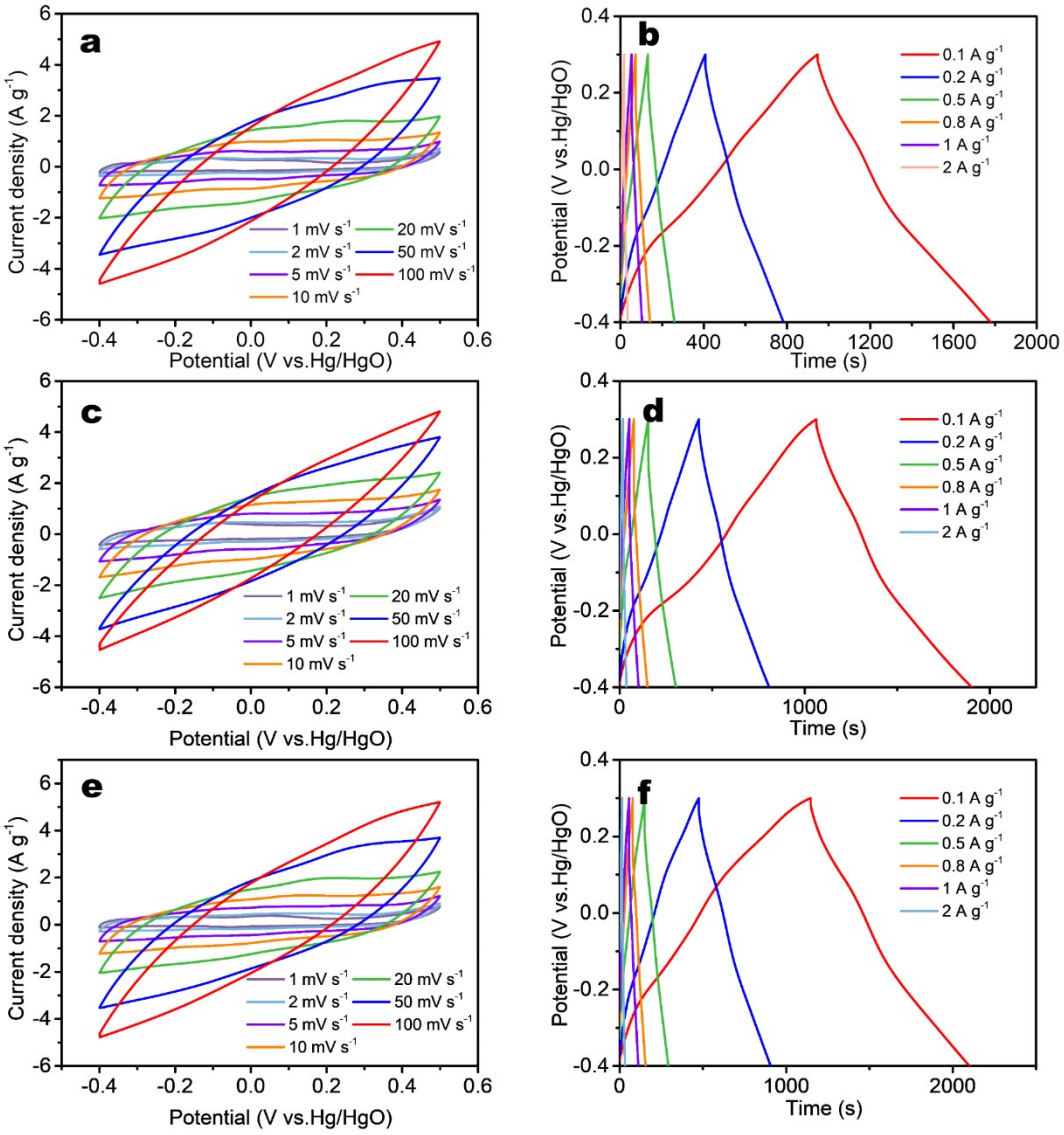

Fig. S15 (a) CV curves of Co@CPE-800 electrode at different scan rates. (b) GCD curves of Co@CPE-800 electrode at different current densities. (c) CV curves of Co@CPE-900 electrode at different scan rates. (d) GCD curves of Co@CPE-900 electrode at different current densities. (e) CV curves of Co@CPE-1000 electrode at different scan rates. (f) GCD curves of Co@CPE-1000 electrode at different current densities.

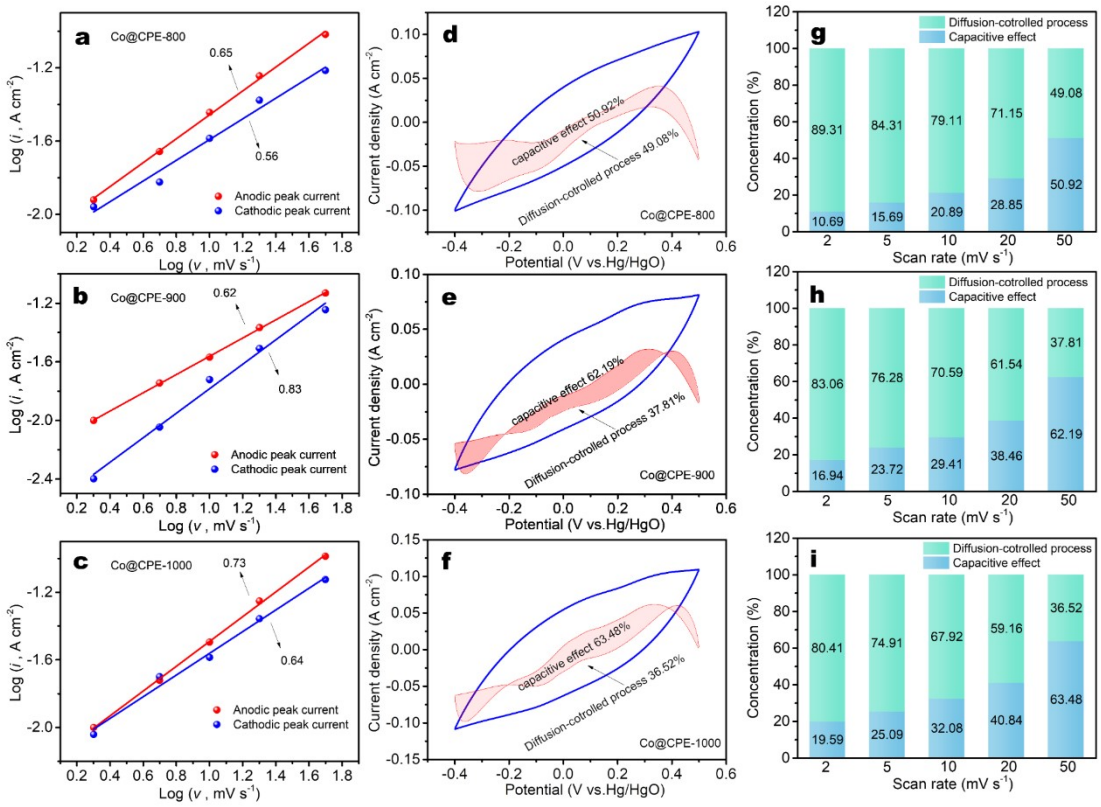

Fig. S16 The plots of i_a and i_c peak current densities as a function of scan rate for the (a) Co@CPE-800, (b) Co@CPE-900, and (c) Co@CPE-1000 electrodes. The contributions of capacitive effect and diffusion-controlled processes to total current for (d) Co@CPE-800, (e) Co@CPE-900, and (f) Co@CPE-1000 electrodes at a scan rate of 50 mV s^{-1}. Contribution of capacitive effect and diffusion-controlled process to the overall areal capacitance for the (g) Co@CPE-800, (h) Co@CPE-900, and (i) Co@CPE-1000 electrodes.

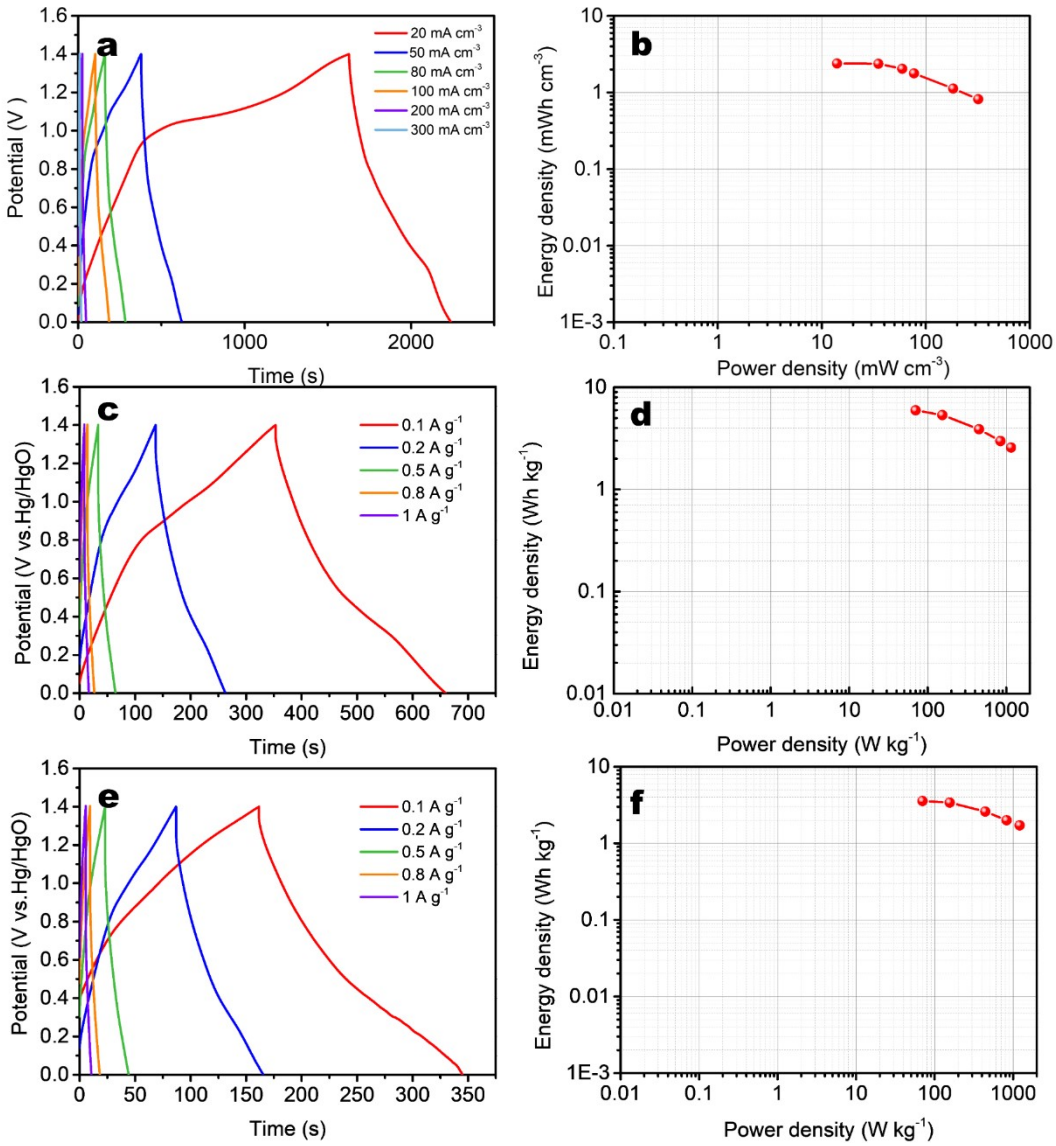

Fig. S17 (a) GCD curves of Co@CPE-1000-based SC at different current densities. (b) Ragone plot of Co@CPE-1000-based SC. (c) GCD curves of Co@CPE-1000-based SC at different current densities. (d) Ragone plot of Co@CPE-1000-based SC. (based on the loading amounts of Co_2P in the electrodes). (e) GCD curves of Co@CPE-1000-based SC at different current densities. (f) Ragone plot of Co@CPE-1000-based SC. (based on the overall mass of the electrodes).

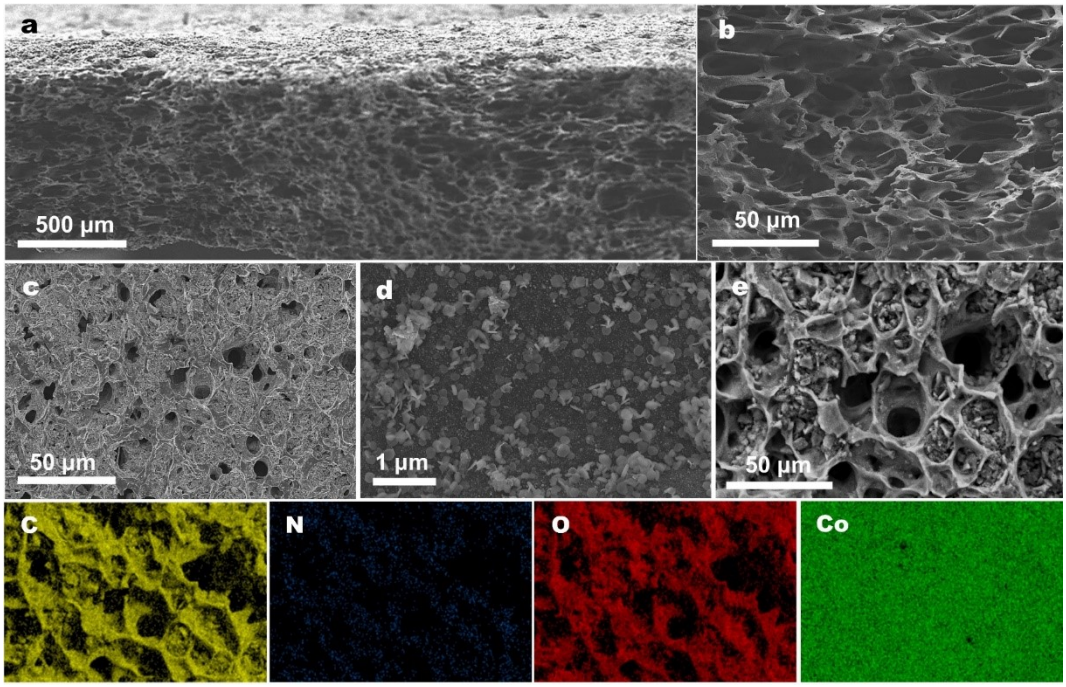

Fig. S18 (a) SEM image showing the overall view of cycled Co@CPE-1000 electrode. (b) Side -view and (c) top-view SEM images of cycled Co@CPE-1000 electrode. (e) High-magnification SEM image of cycled Co@CPE-1000 electrode. (f) SEM image of cycled Co@CPE-1000 electrode and the corresponding elemental mapping images.

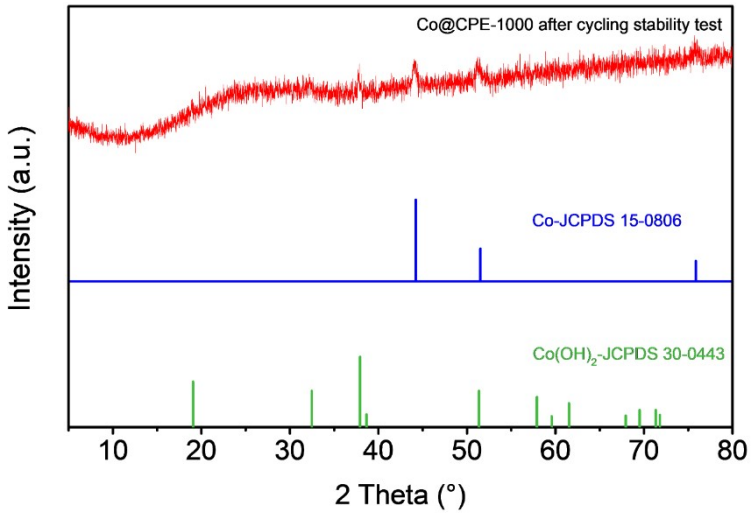

Fig. S19 XRD patterns of Co@CPE-1000 electrode after the cycling stability test.

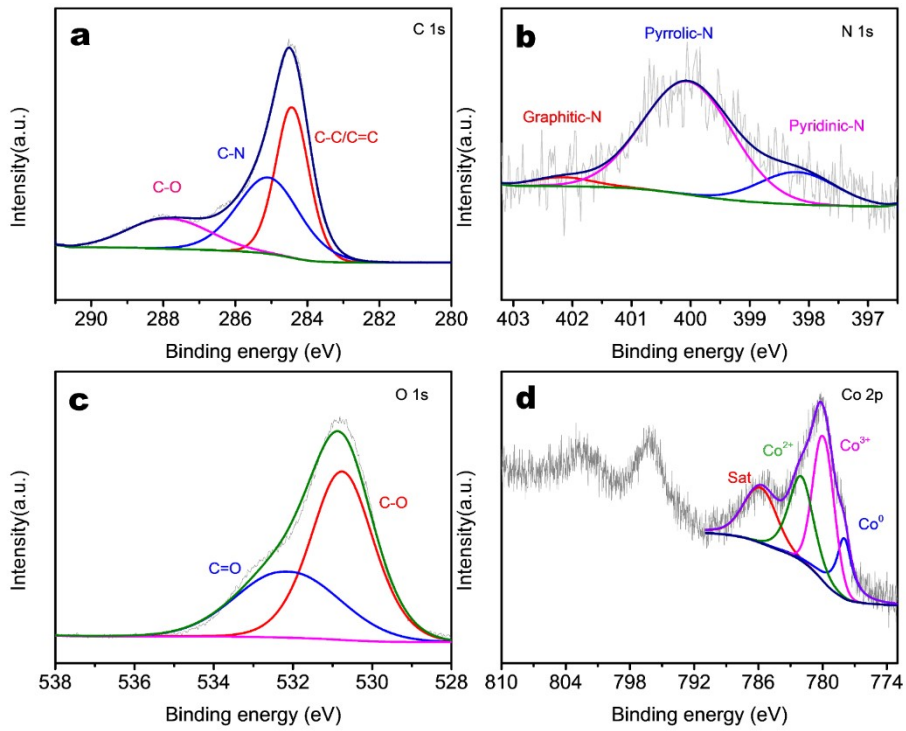

Fig. S20 (a) C 1s, (b) N 1s, (c) O 1s, and (d) Co 2p XPS spectra of the Co@CPE-1000 electrodes after the cycling stability test.

Supplementary references

1 G. L. Zhu, H. Wen, M. Ma, W. Y. Wang, L. Yang, L. C. Wang, X. F. Shi, X. W. Cheng, X. P. Sun and Y. D. Yao, *Chem. Commun.*, 2018, **54**, 10499-10502.

2 C. L. Wang, X. R. Li, W. P. Yang, Y. X. Xu and H. Pang, *Chinese Chem. Lett.*, 2021, **32**, 2909-2913.

3 J. H. Zheng, R. M. Zhang, P. F. Yu and X. G. Wang, *J. Alloy Compd.*, 2019, **772**, 359-365.

4 T. Kshetri, D. D. Khumujam, T. I. Singh, Y. S. Lee, N. H. Kim and J. H. Lee, *Chem. Eng. J.*, 2022, **437**,135338.

5 I. F. Gul, H. Anwar, M. A. Raza, R. Ahmad, N. Iqbal and G. Ali, *J. Ind. Eng. Chem.*, 2022, **116**, 595-605.

6 T. P. Hu, L. L. Gao, W. D. Zhou and J. Zhang, *J. Alloy Compd.*, 2022, **895**,162577.

7 H. L. Wu and J. Q. He, *Diam. Relat. Mater.*, 2022, **123**,108912.

8 B. R. Ye, M. L. Huang, L. Q. Fan, J. M. Lin and J. H. Wu, *J. Alloy Compd.*, 2019, **776**, 993-1001.

9 Y. Song, M. Y. Zhang, T. Y. Liu, T. J. Li, D. Guo and X. X. Liu, *Nanomaterials-Basel*, 2019, **9**, 1110.

10 M. G. Radhika, B. Gopalakrishna, K. Chaitra, L. K. G. Bhatta, K. Venkatesh, M. K. S. Kamath and N. Kathyayini, *Mater. Res. Express.*, 2020, **7**,054003.

11 R. Ramachandran, C. H. Zhao, D. Luo, K. Wang and F. Wang, *Electrochim. Acta*, 2018, **267**, 170-180.